Observation of Genuine Tripartite Non-Gaussian Entanglement from a Superconducting Three-Photon Spontaneous Parametric Down-Conversion Source

Benjamin Jarvis-Frain,[1,*,†] Andy Schang,[1,*] Fernando Quijandría,[2] Ibrahim Nsanzineza,[1] Dmytro Dubyna,[1] C. W. Sandbo Chang,[1,2] Franco Nori,[2,3] and C. M. Wilson[1,‡]

[1]*Institute for Quantum Computing and Department of Electrical and Computer Engineering, University of Waterloo, Waterloo, Ontario N2L 3G1, Canada*
[2]*RIKEN Center for Quantum Computing, RIKEN, Wakoshi, Saitama 351-0198, Japan*
[3]*Physics Department, University of Michigan, Ann Arbor, Michigan 48109-1040, USA*

(Received 8 October 2025; accepted 11 June 2026; published 21 July 2026)

The generation of entangled photons through spontaneous parametric down-conversion (SPDC) is a critical resource for many key experiments and technologies in the domain of quantum optics. Historically, SPDC was limited to the generation of photon pairs. However, the use of the strong nonlinearities in circuit quantum electrodynamics has recently enabled the observation of three-photon SPDC (3P-SPDC). Despite great interest in the entanglement structure of the resultant states, entanglement between photon triplets produced by a 3P-SPDC source has still not been confirmed. Here, we report on the observation of genuine tripartite non-Gaussian entanglement in the steady-state output field of a 3P-SPDC source consisting of a superconducting parametric cavity coupled to a transmission line. We study this non-Gaussian tripartite entanglement using an entanglement witness built from three-mode correlation functions, observing a maximum violation of the bound by 15 standard deviations of the statistical noise. Furthermore, we find strong agreement between the observed and the analytically predicted scaling of the entanglement witness. We then explore the impact of the temporal function used to define the photon mode on the observed value of the entanglement witness.

DOI: 10.1103/4ts4-qj74

The ability to generate entangled pairs of photons via spontaneous parametric down-conversion (SPDC) [1,2] has enabled many achievements in fundamental quantum information science [3–5] and its applications [6–8]. The natural extension of this phenomenon to generating photon triplets from three-photon SPDC (3P-SPDC) was studied theoretically starting over 30 years ago [9,10]. However, 3P-SPDC was only recently demonstrated using superconducting circuits operating at microwave frequencies [11,12]. This development has spurred renewed interest in the phenomenon and its potential applications [13–24]. These theoretical studies predict a variety of useful nonclassical states, depending on the degeneracy of the modes involved. In the case of degenerate 3P-SPDC into a single mode, the resulting trisqueezed state was predicted to exhibit Wigner negativity [10] and can be used to generate approximate cubic phase states, which are themselves non-Gaussian resource states for universal continuous-variable quantum computation [12,25]. Alternatively, in the case of nondegenerate down-conversion into three different modes, the photons have been theoretically shown to exhibit genuine tripartite non-Gaussian entanglement [17,26] and can, for example, be used as a source of heralded two-photon entangled states [27]. These results on 3P-SPDC add to a growing body of work on nonclassical effects in few-photon nonlinear optics [28–32] including recent experimental demonstrations [33–35].

In this Letter, we study the tripartite entanglement of nondegenerate 3P-SPDC into three different modes. In Ref. [36] it was demonstrated that it is impossible to detect tripartite entanglement from 3P-SPDC using only moments of the field quadratures, $\hat{X}$ and $\hat{P}$, up to second order. That is, entanglement in these states cannot be detected using standard measures developed for Gaussian states. Subsequently, it was shown that the entanglement of these states could be detected with higher moments of the quadratures. Consequently, the witness we use to observe this tripartite entanglement is built from moments up to fourth order [26].

Since our entanglement witness depends on the third moments of the quadratures, it certifies that the states found to be entangled are also non-Gaussian (given that the states are mean-zero) [37,38]. For a detailed discussion of this certification, see Supplemental Material [39]. Non-Gaussian entanglement has recently been of great interest in the field of quantum information due to its advantages over Gaussian entanglement in tasks like sensing and metrology [13,51–53]. Furthermore, non-Gaussian entanglement has

[*]These authors contributed equally to this work.
[†]Present address: Rigetti Computing, Berkeley, California 94710, USA.
[‡]Contact author: chris.wilson@uwaterloo.ca

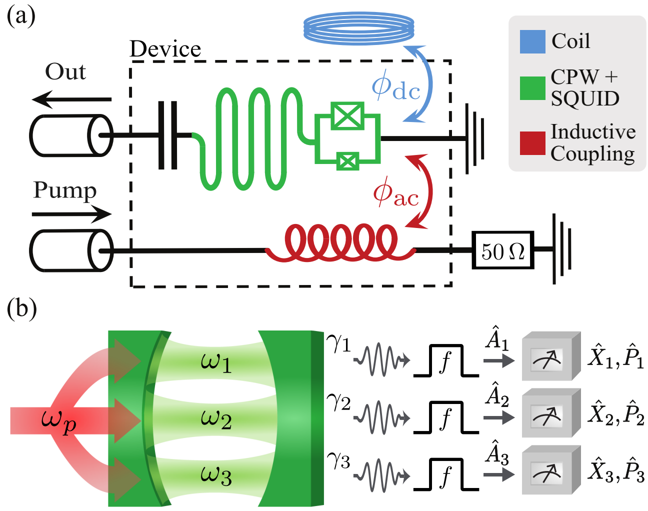

FIG. 1. Three-photon spontaneous parametric down-conversion (3P-SPDC) in a superconducting cavity. (a) Circuit model. The short circuit at one end of a meandered $\lambda/4$ CPW resonator (green) is replaced by an asymmetric SQUID that creates a tunable boundary condition for the resonator modes. The SQUID is flux-coupled to a static dc coil (blue) and an ac pump line (red). The other end of the cavity is capacitively coupled to an output transmission line. (b) Cartoon of 3P-SPDC in the cavity with heterodyne measurement of the three propagating output modes defined by a temporal mode function. High-frequency pump photons (red) are split into entangled photon triplets inside the cavity at distinct frequencies (green), which couple to the continuum of the output line with coupling strengths γ_i. We convert the propagating modes into discrete modes, $\hat{A}_i$, with a temporal mode function $f(t)$, lastly measuring their voltage quadratures $\hat{X}_i$ and $\hat{P}_i$.

been shown to be necessary for quantum advantage in many bosonic quantum computational schemes [54]. For instance, in the continuous-variable cluster state scheme, particular non-Gaussian states are a sufficient resource along with a complete set of Gaussian operations for universal quantum computation [55,56].

We implement nondegenerate 3P-SPDC inside a superconducting microwave cavity consisting of a coplanar waveguide (CPW) terminated by an asymmetric superconducting quantum interference device (SQUID) at one end of the resonator and capacitively coupled to a transmission line at the other, as illustrated in Fig. 1(a) [57–59]. The CPW constituting the resonator is approximately 48 mm long, supporting several modes over our 4- to 12-GHz measurement bandwidth, with the three modes used here being at $\omega_1/2\pi = 5.56$ GHz, $\omega_2/2\pi = 6.83$ GHz, and $\omega_3/2\pi = 7.90$ GHz. We vary the impedance of the line along its length such that the mode frequencies are not equally spaced [11,60–62]. The asymmetric SQUID is inductively coupled to an on-chip microwave pump line, which allows for a time-varying modulation of the flux $\phi_{ac}(t)$, as well as to an off-chip coil, which provides a static flux bias ϕ_{dc}.

The SQUID allows for the flux potential of the cavity to be parametrically modulated in time using the pump line. Furthermore, it has been shown that the asymmetry in the SQUID junctions, together with the correct frequency modulation, leads to the activation of odd-order terms in the Hamiltonian of the system [11,63,64]. The flux across the SQUID at the cavity termination is related to the bosonic operators of the cavity modes by $\hat{\Phi} = \sum_i \Phi_i(\hat{a}_i + \hat{a}_i^\dagger)$, where Φ_i is the scale of zero-point fluctuations of the flux of the i_{th} mode across the SQUID. The junction potential can be written as $\hat{H}_{\mathrm{even}}(\hat{\phi}, t) + \hat{H}_{\mathrm{odd}}(\hat{\phi}, t)$, where $\phi = 2\pi\Phi/\Phi_0$ and Φ_0 is the flux quantum. Here, $\hat{H}_{\mathrm{even}}$ is the potential of a symmetric SQUID $\hat{H}_{\mathrm{even}}(\hat{\phi}, t) = -E_+ \cos[\phi_{\mathrm{ext}}(t)] \cos\hat{\phi}$, where E_+ is the sum of the Josephson energies of both junctions and $\phi_{\mathrm{ext}}(t) = \phi_{\mathrm{dc}} + \phi_{\mathrm{ac}}(t)$ is the total external flux threading the SQUID. The contribution due to the junction asymmetry is $\hat{H}_{\mathrm{odd}} = -E_- \sin[\phi_{\mathrm{ext}}(t)] \sin\hat{\phi}$, where E_- is the difference between the junctions' Josephson energies. The lowest nonlinear contribution to the odd terms is $\hat{H}_{\mathrm{odd}} \propto \phi_{\mathrm{ac}}(t) E_- \sin\hat{\phi}$. Restricting to just three resonant modes of the cavity, the Hamiltonian term accounting for the three-photon interaction is

$$\hat{H}_{\mathrm{odd}} = \hbar g_0(\alpha e^{i\omega_p t} + \alpha^* e^{-i\omega_p t}) \times (\hat{a}_1 + \hat{a}_1^\dagger)(\hat{a}_2 + \hat{a}_2^\dagger)(\hat{a}_3 + \hat{a}_3^\dagger), \quad (1)$$

where g_0 is a coupling constant dictated by the SQUID asymmetry as well as ϕ_{dc}, and α is the complex amplitude of the pump field. Finally, as is typical in circuit QED setups, there are residual Kerr interactions between the modes due to the time-independent part of $\hat{H}_{\mathrm{even}}$.

By pumping at the sum frequency of the three cavity modes, that is $\omega_p = \omega_1 + \omega_2 + \omega_3$, we obtain the following total Hamiltonian in an interaction frame after using a rotating-wave approximation:

$$\hat{H} = \hbar g(\hat{a}_1\hat{a}_2\hat{a}_3 + \hat{a}_1^\dagger\hat{a}_2^\dagger\hat{a}_3^\dagger) - \sum_{n,m} \chi_{nm}\hat{a}_n^\dagger\hat{a}_m^\dagger\hat{a}_n\hat{a}_m, \quad (2)$$

where we have included the Kerr terms with strengths χ_{nm}. In addition, $g = g_0\alpha$ is the effective three-photon interaction strength in the parametric approximation with our attention restricted to real values of α.

A witness that could observe the tripartite entanglement of states generated by 3P-SPDC was proposed in Ref. [26]. This witness follows from Cauchy-Schwarz–derived inequalities introduced in Refs. [65,66]. A similar witness was derived earlier in [67] by generalizing the method of matrices of moments of field operators introduced in [68], and further extended in [69]. Subsequently, other witnesses have been proposed, all of which use moments of the field operators of third order and higher [13,15,21,70].

The witnesses described in [13] and [21] detect entanglement, respectively, in terms of the quantum Fisher information and the capacity for quantum steering, both of which are appealing in that they measure entanglement through quantities directly connected to practical utility. However, we operate in the few-photon regime, where the thermal background is small but not negligible. For these reasons, we restrict to the original witness for genuine tripartite entanglement [26]

$$W = |\langle \hat{a}_1 \hat{a}_2 \hat{a}_3 \rangle| - \sum_{\substack{i,j,k=1,2,3 \\ i\neq j\neq k\neq i}} \sqrt{\langle \hat{n}_i \rangle \langle \hat{n}_j \hat{n}_k \rangle}, \qquad (3)$$

where $\hat{n}_i = \hat{a}_i^\dagger \hat{a}_i$ is the number operator on the i_{th} mode. We note that this witness certifies both the weaker *full inseparability* and stronger *genuine multipartite entanglement*. For a detailed discussion of the distinction, see, e.g., Ref. [26].

Experimentally, the entangled photon triplets generated from 3P-SPDC inside the cavity leak into the capacitively coupled transmission line, where we measure them using a linear amplifier as illustrated in Fig. 1(b). Following digitization, we compute moments of the quadrature voltages of the propagating states [71]. In this Letter, we focus on measuring the entanglement directly in the propagating states, as opposed to reconstructing the entanglement in the cavity. In addition to being more experimentally accessible, tripartite entanglement in propagating states may also be a more practical form of nonclassical resource for applications like quantum-enhanced metrology and remote sensing [13,19].

In general, the propagating states in the transmission line are described by continuum operators, e.g., in the time domain as $\hat{a}_{\mathrm{out},i}(t)$, where i denotes the corresponding cavity mode. To analyze the correlations in the system, we reduce the continuum operators to single-mode operators, by defining appropriate mode functions [72,73]. In particular, we use a time domain description, as spectral analysis of higher-order quantum correlation functions (beyond the spectral density) is not well developed. The discrete bosonic operator annihilating a photon occupying the mode defined by the function $f(t)$ is $\hat{A}_i = \int \mathrm{d}t\, f(t) \hat{a}_{\mathrm{out},i}(t)$. The normalization condition $\int_0^\infty \mathrm{d}t |f(t)|^2 = 1$ guarantees that the discretized modes obey the bosonic commutation relation $[\hat{A}_i, \hat{A}_j^\dagger] = \delta_{ij}$. Here, we use the same function, $f(t)$, to filter all three modes, because we found no clear advantage to using different functions for each mode (see Supplemental Material [39]). Although our rf digitizers have built-in antialiasing filters, we can control the mode function used in the experiments by oversampling the data and then digitally filtering with the chosen mode function. In this Letter we investigate the steady-state emission from the continuously driven cavity by only filtering the output emission once the cavity field has reached a stationary regime.

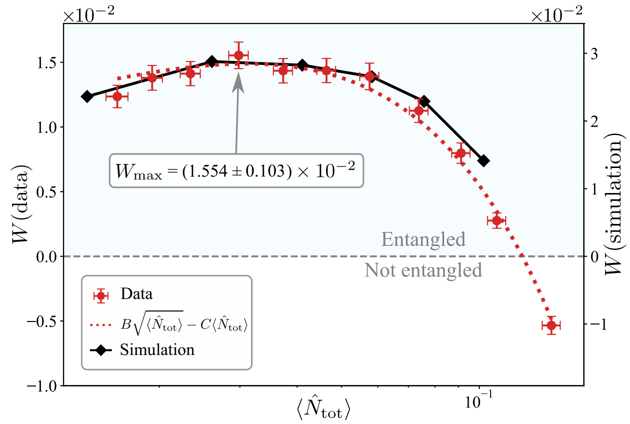

FIG. 2. Measured entanglement witness, W, for three-mode states generated from 3P-SPDC as a function of their measured average photon number, $\langle \hat{N}_{\mathrm{tot}} \rangle$, which is varied by changing the pump amplitude. The error bars show one standard deviation of statistical error, σ, above and below the mean. We observe $W > 0$, indicating genuine tripartite non-Gaussian entanglement, over nearly an order of magnitude of $\langle \hat{N}_{\mathrm{tot}} \rangle$ before entanglement is no longer detected. At the maximum value of W, we violate the bound by more than 15σ. We compare the measured witness values against stochastic trajectories simulations and an analytically predicted scaling law, Eq. (7). Simulation results are plotted on the right axis, rescaled by a fitted factor of 1.9.

In our measurements, the propagating states are first amplified by a traveling-wave parametric amplifier (TWPA), followed by a sequence of HEMT amplifiers. They are then measured using heterodyne detection with three room-temperature rf digitizers. The image band of each digitizer is rejected using an external superheterodyne mixing stage on each channel. The moments of the voltage quadratures of the states as they leave the cavity are reconstructed by calibrating the gain and noise of the amplifier chain using a shot noise tunnel junction provided by NIST Boulder. We measure the moments of the amplifier noise by taking interleaved measurements of the output signals with the down-conversion process on and off. Finally, we calibrate the measurement and parametric pump frequencies to account for the external flux dependence and Kerr terms in the SQUID potential that shift the cavity mode frequencies with pump power (see Supplemental Material [39]). Specifically, the pump frequency ranges from 20.293 to 20.292 GHz as the pump is increased from the weakest to the strongest power.

In Fig. 2, we plot the measured value of W as a function of the total average number of photons in the observed state, $\langle \hat{N}_{\mathrm{tot}} \rangle = \langle \hat{N}_1 \rangle + \langle \hat{N}_2 \rangle + \langle \hat{N}_3 \rangle$, which is controlled by the pump strength. The temporal mode is fixed by a 1-MHz antialiasing filter built into the digitizers' firmware, which corresponds to a windowed sinc function in the time domain (see Supplemental Material [39]). Entanglement is observed over nearly an order of magnitude of $\langle \hat{N}_{\mathrm{tot}} \rangle$, with an observed maximum value of $W = (1.554 \pm 0.103) \times 10^{-2}$, violating the entanglement bound by 15 standard deviations of the

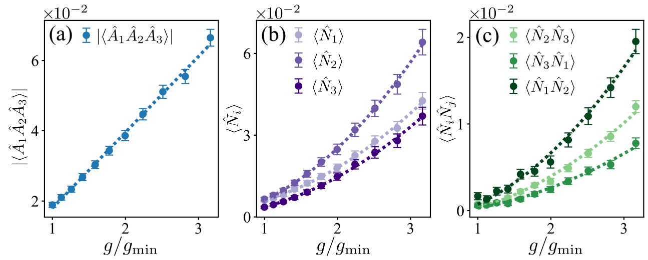

FIG. 3. Measured correlators as a function of the normalized three-photon drive strength, $g/g_{\min}$. We estimate $g_{\min} = 0.057$ MHz (see Supplemental Material [39]). Dotted lines are the linear (a) and quadratic (b),(c) scalings of the correlators predicted by perturbation theory in Eqs. (4)–(6) with fitted multiplicative factors.

statistical noise. We note that $\langle \hat{N}_\mathrm{i}\rangle$ are photons per mode. However, we detect a stream of these modes with a repetition rate equal to our measurement bandwidth. Therefore, $\langle \hat{N}_\mathrm{tot}\rangle = 0.1$ corresponds to a photon flux of $\sim 10^5$ photons/s in our 1-MHz bandwidth.

To understand the behavior of W, we show the measured filtered output field correlators, which contribute to the entanglement witness as a function of the normalized three-photon drive strength $g/g_{\min}$ in Fig. 3. The measured value of $\langle \hat{N}_\mathrm{tot}\rangle \lesssim 0.2$ places us in a weak driving regime, which can be studied analytically using perturbation theory. As detailed in Supplemental Material [39], we treat the three-photon Hamiltonian as a small perturbation to the undriven dissipative dynamics, which cools the three-mode cavity system to a thermal state close to the photon vacuum $\hat{\rho}_\mathrm{ss}^{(0)} \approx |000\rangle\langle 000|$. Our perturbative parameter is $\lambda = g/\gamma_T$, where γ_T is the sum of the total decay rates of the three cavity modes, $\gamma_T = \sum_i \gamma_i$. We neglect Kerr nonlinearities in our analysis as they have minimal effect in the few-photon regime. Up to second order in λ, the cavity steady-state is expressed as $\hat{\rho}_\mathrm{ss} \approx \hat{\rho}_\mathrm{ss}^{(0)} + \lambda\hat{\rho}_\mathrm{ss}^{(1)} + \lambda^2\hat{\rho}_\mathrm{ss}^{(2)}$. The first-order correction to the steady-state $\hat{\rho}_\mathrm{ss}^{(1)} \propto \lambda|111\rangle\langle 000| + \mathrm{H.c.}$ is solely responsible for the three-photon correlations $\langle \hat{a}_1\hat{a}_2\hat{a}_3\rangle$, while terms contributing to the modes' populations $\langle \hat{n}_i\rangle$ and number-number correlations $\langle \hat{n}_i\hat{n}_j\rangle$ only appear in the second-order correction to the steady-state. The explicit relations for the lowest-order contributions to the steady-state cavity field correlations are

$$|\langle \hat{a}_1\hat{a}_2\hat{a}_3\rangle| = \frac{2g}{\gamma_T} \tag{4}$$

$$\langle \hat{n}_i\rangle = \left(\frac{2g}{\gamma_T}\right)^2\left(\frac{\gamma_T}{\gamma_i}\right) \tag{5}$$

$$\langle \hat{n}_i\hat{n}_j\rangle = \left(\frac{2g}{\gamma_T}\right)^2\left(\frac{\gamma_T}{\gamma_i+\gamma_j}\right). \tag{6}$$

Starting from our steady-state approximation it is possible to calculate different order multitime correlations and, from these, the output field correlations. As shown in Supplemental Material [39], the above leading order corrections to the different correlators map to the output field, with the explicit relations depending on the particular temporal mode profile $f(t)$. This agrees with the scaling observed in Fig. 3, that is $|\langle \hat{A}_1\hat{A}_2\hat{A}_3\rangle| \propto g$, while $\langle \hat{N}_i\rangle, \langle \hat{N}_i\hat{N}_j\rangle \propto g^2$. Owing to these scaling laws and the definition of the entanglement witness (3), in the weak driving regime we have that $W \propto g$. Therefore, independent of the total decay rate, an arbitrarily weak but nonzero value of g suffices to generate genuine tripartite entanglement in our system, which agrees with what we observe in Fig. 2.

By inverting these proportionalities and isolating for $\langle \hat{N}_\mathrm{tot}\rangle$, we can predict a scaling law for W (see Supplemental Material [39]),

$$W = B\sqrt{\langle \hat{N}_\mathrm{tot}\rangle} - C\langle \hat{N}_\mathrm{tot}\rangle, \tag{7}$$

where B and C are constants. Using B and C as free parameters, we fit this relation to the data in Fig. 2, observing excellent agreement. We see then that the witness detects entanglement when the output is dominated by third-order correlations, but gradually fails as the even-order correlations grow. We speculate that witnesses based on higher-order correlators, such as [21,70], might be able to detect entanglement at higher pump powers, but testing this experimentally is a topic for future work.

To go beyond the weak-driving regime we use the input-output method with quantum pulses [74]. Following this, we derive a master equation to study the dynamics of the three resonator modes together with the three filtered output modes. Here, each propagating output wave packet is treated as a single mode of an auxiliary fictitious resonator. We solve numerically the dynamics of six bosonic modes using QuTiP [75]. In the Supplemental Material [39] we provide more details on this method and benchmark the numerical simulations against analytical results in the weak-driving regime. We also include Kerr nonlinearities, which we measure using a calibrated measurement of the cavity Kerr shifts.

We can directly compare the simulated entanglement witness value against that observed experimentally by setting the temporal profile of the propagating mode in the simulations to match the antialiasing filter of the digitizers and sweeping over the same range of drive strengths, g. Since g is not an experimentally accessible parameter, we estimate it by fitting the lowest order nonzero correlators $\langle \hat{N}_i\rangle$, in simulations to those observed experimentally, and find that g is within 0.057 and 0.181 MHz (see Supplemental Material [39]). The numerically calculated witness values are shown in Fig. 2 as the

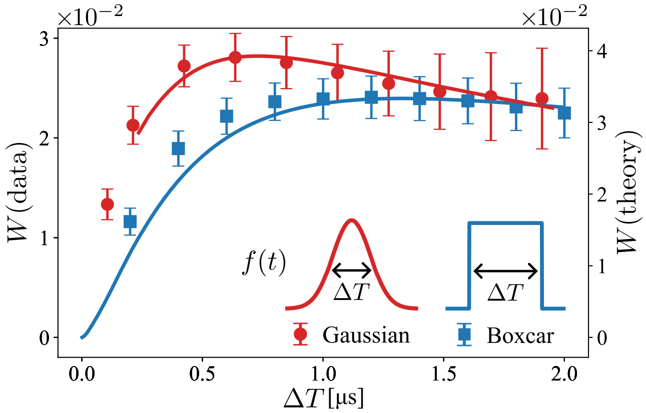

FIG. 4. Entanglement witness, W, as a function of width, ΔT, of the temporal mode function for Gaussian (red) and boxcar (blue) mode functions. Markers are experimental data, and solid lines are theoretical predictions. The width of the Gaussian mode function is defined as the full-width-half-maximum value, while the boxcar width is defined by the edges of the boxcar. W grows rapidly for small ΔT, until it reaches a maximum. The maximum values are achieved when ΔT is significantly larger than the cavity lifetimes (0.12–0.25 μs). We see that larger values of W are obtained with the Gaussian mode function, in agreement with previous works [77,78].

solid black line. Although the simulated value of W quantitatively disagrees by a multiplicative factor of 1.9, the qualitative form is reproduced well and is in agreement with the analytical scaling predictions. Although we can improve the quantitative agreement by allowing additional free parameters, such as the pump detuning, to vary in the simulations, we felt it better to show the level of agreement with as many parameters as possible fixed at their independently measured and calibrated values. Given the experimental and theoretical complexity of the system, we find the agreement to be quite good.

To explore the nontrivial dependence of W on the multimodal structure of the output state [76], we test two types of temporal mode functions. To do this experimentally, we first oversample the data with a large sampling frequency, and then digitally filter with the mode function of our choice. In the continuous pumping regime, discretization is implemented as a convolution of the measured quadrature voltages with the chosen temporal mode function (see Supplemental Material [39]). We use a boxcar as a simple reference function and compare it to a Gaussian function, which was shown in [77] to reveal stronger nonclassical properties when studying the output state of a Kerr parametric oscillator.

The entanglement witness value as a function of temporal mode widths for both boxcar and Gaussian functions is shown in Fig. 4. For both functions, the witness grows to a maximum when the width is several times the average cavity lifetime of 0.17 μs, then drops off for wider functions. Similar to the parametric oscillator in [77], the observed entanglement witness is larger for Gaussian modes and peaks at a width around 5 times the average cavity lifetime. Although W is not an entanglement monotone, and therefore does not necessarily measure the strength of the entanglement, we can infer that the relative magnitude of the tripartite correlations in our propagating mode reaches an optimum value at a finite width of temporal modes. This can be understood as the mode with the highest probability of capturing the emission of all three photons in a triplet into the transmission line.

The Gaussian entanglement generated by two-photon SPDC has been a key enabling technology for many experimental achievements in quantum information. The unique entanglement structure generated from non-Gaussian processes offers to expand these capabilities and enable novel applications and experiments in this domain. Among its nonclassical behaviors, the non-Gaussian tripartite entanglement of nondegenerate 3P-SPDC heralds its potential importance for quantum metrology [13], probing the fundamentals of entanglement [18,20], and even studying models of quantum gravity [79]. Integrating this device with superconducting qubits has been proposed to enable swapping of the non-Gaussian entanglement between bosonic oscillator modes and qubit modes [80]. Furthermore, marginal improvements to the temperature of the cavity could enable the observation of the metrological advantage predicted in [13]. Our results open new avenues for exploring quantum states of light involving non-Gaussian entanglement in a continuous-variable system by leveraging the unique characteristics of 3P-SPDC in microwave quantum optics.

Acknowledgments—We thank Nicolai Friis, Marcus Huber, and Carlos Sabín for important discussions on the proper choice of witness. We thank QuantWare for providing the Crescendo TWPA used to amplify our triplet states. We thank Joe Aumentado and the Advanced Microwave Photonics Group (686.05) at the National Institute of Standards and Technology (Boulder) for providing the shot noise tunnel junction device used for calibration. We further thank Joe Aumentado and Maxime Malnou at NIST for useful discussions on performing broadband calibrations. C. M. W., B. J.-F., A. S., I. N., C. W. S. C., and D. D. acknowledge the Canada First Research Excellence Fund (CFREF); NSERC of Canada; the Canadian Foundation for Innovation; the Ontario Ministry of Research and Innovation; Defense Research and Development Canada; Industry Canada; and the Innovation for Defence Excellence and Security (IDEaS) program from the Canadian Department of National Defence (DND) for financial support. F. N. is supported in part by: the Japan Science and Technology Agency (JST) [via the CREST Quantum Frontiers program Grant No. JPMJCR24I2, the Quantum Leap Flagship Program (Q-LEAP), and the Moonshot R&D Grant No. JPMJMS2061], and the Office of Naval Research (ONR) Global (via Grant No. N62909-23-1-2074).

Data availability—The data that support the findings of this article are not publicly available upon publication because it is not technically feasible and/or the cost of preparing, depositing, and hosting the data would be prohibitive within the terms of this research project. The data are available from the authors upon reasonable request.

[1] D. C. Burnham and D. L. Weinberg, Phys. Rev. Lett. **25**, 84 (1970).
[2] M. O. Scully and M. S. Zubairy, *Quantum Optics* (Cambridge University Press, Cambridge, England, 1997).
[3] M. D. Reid, Phys. Rev. A **40**, 913 (1989).
[4] W. Tittel, J. Brendel, H. Zbinden, and N. Gisin, Phys. Rev. Lett. **81**, 3563 (1998).
[5] S. Friberg, C. K. Hong, and L. Mandel, Phys. Rev. Lett. **54**, 2011 (1985).
[6] A. Lyons, G. C. Knee, E. Bolduc, T. Roger, J. Leach, E. M. Gauger, and D. Faccio, Sci. Adv. **4**, eaap9416 (2018).
[7] J. Yin *et al.*, Nature (London) **582**, 501 (2020).
[8] E. Martín-López, A. Laing, T. Lawson, R. Alvarez, X.-Q. Zhou, and J. L. O'Brien, Nat. Photonics **6**, 773 (2012).
[9] S. L. Braunstein and R. I. McLachlan, Phys. Rev. A **35**, 1659 (1987).
[10] K. Banaszek and P. L. Knight, Phys. Rev. A **55**, 2368 (1997).
[11] C. W. Sandbo Chang, C. Sabín, P. Forn-Díaz, F. Quijandría, A. M. Vadiraj, I. Nsanzineza, G. Johansson, and C. M. Wilson, Phys. Rev. X **10**, 011011 (2020).
[12] A. M. Eriksson, T. Sépulcre, M. Kervinen, T. Hillmann, M. Kudra, S. Dupouy, Y. Lu, M. Khanahmadi, J. Yang, C. Castillo-Moreno, P. Delsing, and S. Gasparinetti, Nat. Commun. **15**, 2512 (2024).
[13] M. Tian, Y. Xiang, F.-X. Sun, M. Fadel, and Q. He, Phys. Rev. Appl. **18**, 024065 (2022).
[14] P. Laha, D. W. Moore, and R. Filip, Phys. Rev. Lett. **132**, 210201 (2024).
[15] D. Zhang, Y. Cai, Z. Zheng, D. Barral, Y. Zhang, M. Xiao, and K. Bencheikh, Phys. Rev. A **103**, 013704 (2021).
[16] D. Zhang, D. Barral, Y. Cai, Y. Zhang, M. Xiao, and K. Bencheikh, Phys. Rev. Lett. **127**, 150502 (2021).
[17] D. Zhang, D. Barral, Y. Zhang, M. Xiao, and K. Bencheikh, Phys. Rev. Lett. **130**, 093602 (2023).
[18] M. Wei, H. Tan, and Q. He, Quantum Sci. Technol. **7**, 045021 (2022).
[19] D. Barral, M. Isoard, G. Sorelli, M. Gessner, N. Treps, and M. Walschaers, New J. Phys. **26**, 083012 (2024).
[20] T. H. Chen, Y. B. Yu, and A. X. Chen, Phys. Rev. A **106**, L060601 (2022).
[21] M. Wei and H. Tan, Phys. Rev. A **110**, 023729 (2024).
[22] D. Zhang and Z. Ren, Commun. Theor. Phys. **75**, 105101 (2023).
[23] D. Zhang, Y. Zhang, and J. Gao, Phys. Rev. A **112**, 033701 (2025).
[24] M. Banic, M. Liscidini, and J. E. Sipe, Phys. Rev. A **106**, 013710 (2022).
[25] Y. Zheng, O. Hahn, P. Stadler, P. Holmvall, F. Quijandría, A. Ferraro, and G. Ferrini, PRX Quantum **2**, 010327 (2021).
[26] A. Agustí, C. W. Sandbo Chang, F. Quijandría, G. Johansson, C. M. Wilson, and C. Sabín, Phys. Rev. Lett. **125**, 020502 (2020).
[27] A. A. Hnilo, Phys. Rev. A **71**, 033820 (2005).
[28] L. Garziano, V. Macrì, R. Stassi, O. Di Stefano, F. Nori, and S. Savasta, Phys. Rev. Lett. **117**, 043601 (2016).
[29] A. F. Kockum, A. Miranowicz, V. Macrì, S. Savasta, and F. Nori, Phys. Rev. A **95**, 063849 (2017).
[30] R. Stassi, V. Macrì, A. F. Kockum, O. Di Stefano, A. Miranowicz, S. Savasta, and F. Nori, Phys. Rev. A **96**, 023818 (2017).
[31] R. Stassi, S. Savasta, L. Garziano, B. Spagnolo, and F. Nori, New J. Phys. **18**, 123005 (2016).
[32] A. F. Kockum, V. Macrì, L. Garziano, S. Savasta, and F. Nori, Sci. Rep. **7**, 5313 (2017).
[33] S.-P. Wang, A. Mercurio, A. Ridolfo, Y. Wang, M. Chen, T. Li, F. Nori, S. Savasta, and J. Q. You, Nat. Commun. **16**, 8730 (2025).
[34] A. Tomonaga, R. Stassi, H. Mukai, F. Nori, F. Yoshihara, and J. S. Tsai, Nat. Commun. **16**, 5294 (2025).
[35] D. Fraudet, I. Snyman, D. M. Basko, S. Léger, T. Sépulcre, A. Ranadive, G. Le Gal, A. Torras-Coloma, W. Guichard, S. Florens, and N. Roch, Phys. Rev. Lett. **134**, 013804 (2025).
[36] E. A. Rojas González, A. Borne, B. Boulanger, J. A. Levenson, and K. Bencheikh, Phys. Rev. Lett. **120**, 043601 (2018).
[37] G. S. Agarwal, *Quantum Optics* (Cambridge University Press, Cambridge, England, 2012).
[38] S. L. Braunstein and P. van Loock, Rev. Mod. Phys. **77**, 513 (2005).
[39] See Supplemental Material at http://link.aps.org/supplemental/10.1103/4ts4-qj74 for a discussion on certifying that the observed state is non-Gaussian, technical details on the experimental setup and the absolute system calibration, error analysis, and an explanation of the analytical model and numerical simulations, which includes Refs. [40–50].
[40] A. V. Oppenheim, R. W. Schafer, and J. R. Buck, *Discrete-Time Signal Processing*, 2nd ed. (Prentice-Hall, Englewood Cliffs, 1999).
[41] C. Eichler, Experimental characterization of quantum microwave radiation and its entanglement with a superconducting qubit, Ph.D. thesis, ETH Zurich, 2013.
[42] C. Eichler, D. Bozyigit, C. Lang, L. Steffen, J. Fink, and A. Wallraff, Phys. Rev. Lett. **106**, 220503 (2011).
[43] L. Spietz, K. W. Lehnert, I. Siddiqi, and R. J. Schoelkopf, Science **300**, 1929 (2003).
[44] S. Chang, J. Aumentado, W. Wong, and J. C. Bardin, in *2016 IEEE MTT-S International Microwave Symposium (IMS)* (IEEE, San Francisco, CA, 2016), pp. 1–4.
[45] M. Malnou, T. F. Q. Larson, J. D. Teufel, F. Lecocq, and J. Aumentado, Rev. Sci. Instrum. **95**, 034703 (2024).
[46] L. Spietz, R. J. Schoelkopf, and P. Pari, Appl. Phys. Lett. **89**, 183123 (2006).
[47] M. Esposito, A. Ranadive, L. Planat, S. Leger, D. Fraudet, V. Jouanny, O. Buisson, W. Guichard, C. Naud, J. Aumentado, F. Lecocq, and N. Roch, Phys. Rev. Lett. **128**, 153603 (2022).
[48] C. W. Gardiner and M. J. Collett, Phys. Rev. A **31**, 3761 (1985).

[49] B. M. Villegas-Martínez, F. Soto-Eguibar, and H. M. Moya-Cessa, Adv. Math. Phys. **2016**, 9265039 (2016).
[50] J. Combes, J. Kerckhoff, and M. Sarovar, Adv. Phys. X **2**, 784 (2017).
[51] L. Fan and M. S. Zubairy, Phys. Rev. A **98**, 012319 (2018).
[52] H. Zhang, Y. Xia, W. Ye, S. Chang, and Z. Liao, Phys. Rev. A **109**, 062440 (2024).
[53] R. Gallego Torromé, Adv. Quantum Technol. **4**, 2100101 (2021).
[54] U. Chabaud and M. Walschaers, Phys. Rev. Lett. **130**, 090602 (2023).
[55] R. Raussendorf and H. J. Briegel, Phys. Rev. Lett. **86**, 5188 (2001).
[56] M. Gu, C. Weedbrook, N. C. Menicucci, T. C. Ralph, and P. van Loock, Phys. Rev. A **79**, 062318 (2009).
[57] C. M. Wilson, G. Johansson, A. Pourkabirian, M. Simoen, J. R. Johansson, T. Duty, F. Nori, and P. Delsing, Nature (London) **479**, 376 (2011).
[58] K. M. Sundqvist, S. Kintaş, M. Simoen, P. Krantz, M. Sandberg, C. M. Wilson, and P. Delsing, Appl. Phys. Lett. **103**, 102603 (2013).
[59] M. Simoen, C. W. S. Chang, P. Krantz, J. Bylander, W. Wustmann, V. Shumeiko, P. Delsing, and C. M. Wilson, J. Appl. Phys. **118**, 154501 (2015).
[60] C. W. Sandbo Chang, M. Simoen, J. Aumentado, C. Sabín, P. Forn-Díaz, A. M. Vadiraj, F. Quijandría, G. Johansson, I. Fuentes, and C. M. Wilson, Phys. Rev. Appl. **10**, 044019 (2018).
[61] Jimmy S. C. Hung, J. H. Busnaina, C. W. Sandbo Chang, A. M. Vadiraj, I. Nsanzineza, E. Solano, H. Alaeian, E. Rico, and C. M. Wilson, Phys. Rev. Lett. **127**, 100503 (2021).
[62] H. Alaeian, C. W. S. Chang, M. V. Moghaddam, C. M. Wilson, E. Solano, and E. Rico, Phys. Rev. A **99**, 053834 (2019).
[63] I. Svensson, A. Bengtsson, J. Bylander, V. Shumeiko, and P. Delsing, Appl. Phys. Lett. **113**, 022602 (2018).
[64] I. M. Svensson, A. Bengtsson, P. Krantz, J. Bylander, V. Shumeiko, and P. Delsing, Phys. Rev. B **96**, 174503 (2017).
[65] M. Hillery and M. S. Zubairy, Phys. Rev. Lett. **96**, 050503 (2006).
[66] M. Hillery, H. T. Dung, and H. Zheng, Phys. Rev. A **81**, 062322 (2010).
[67] A. Miranowicz, M. Piani, P. Horodecki, and R. Horodecki, Phys. Rev. A **80**, 052303 (2009).
[68] E. Shchukin and W. Vogel, Phys. Rev. A **74**, 030302(R) (2006).
[69] A. Miranowicz, M. Bartkowiak, X. Wang, Y.-x. Liu, and F. Nori, Phys. Rev. A **82**, 013824 (2010).
[70] S. Ma, D. Zhang, Y. Zhao, Y. Yu, G. Jin, and A. Chen, Phys. Lett. A **532**, 130195 (2025).
[71] M. P. da Silva, D. Bozyigit, A. Wallraff, and A. Blais, Phys. Rev. A **82**, 043804 (2010).
[72] K. J. Blow, R. Loudon, Simon J. D. Phoenix, and T. J. Shepherd, Phys. Rev. A **42**, 4102 (1990).
[73] M. G. Raymer and I. A. Walmsley, Phys. Scr. **95**, 064002 (2020).
[74] A. H. Kiilerich and K. Mølmer, Phys. Rev. Lett. **123**, 123604 (2019).
[75] N. Lambert, E. Giguère, P. Menczel, B. Li, P. Hopf, G. Suárez, M. Gali, J. Lishman, R. Gadhvi, R. Agarwal, A. Galicia, N. Shammah, P. Nation, J. R. Johansson, S. Ahmed, S. Cross, A. Pitchford, and F. Nori, Phys. Rep. **1153**, 1 (2026).
[76] M. Khanahmadi, M. M. Lund, K. Mølmer, and G. Johansson, Phys. Rev. Res. **5**, 043071 (2023).
[77] I. Strandberg, G. Johansson, and F. Quijandría, Phys. Rev. Res. **3**, 023041 (2021).
[78] Y. Lu, I. Strandberg, F. Quijandría, G. Johansson, S. Gasparinetti, and P. Delsing, Phys. Rev. Lett. **126**, 253602 (2021).
[79] P. G. C. Rufo, A. Mazumdar, and C. Sabín, Phys. Rev. A **111**, 022444 (2025).
[80] A. A. Casado and C. Sabín, Phys. Rev. A **105**, 022401 (2022).